CHEMISTRY OF MATERIALS

pubs.acs.org/cm

Article

Injectable In Situ Forming Double-Network Hydrogel To Enhance Transplanted Cell Viability and Retention

Xiaoya Ding, Ye Wang, Jiaying Liu, Peng Zhang, Gao Li,* Tianmeng Sun,* and Chunsheng Xiao*

Cite This: *Chem. Mater.* 2021, 33, 5885−5895

Read Online

ACCESS | Metrics & More | Article Recommendations | Supporting Information

ABSTRACT: Cell transplantation by injection has emerged as a promising strategy for the treatment of several diseases and injuries throughout the body. However, the therapeutic efficacy is hampered by the inevitable cell death during mechanical injection, low cell retention at the injection site, and lack of structural support for long-term survival and functioning of the transplanted cells. Till date, no hydrogel formulation exists that can address all of these issues accompanying cell transplantation. Herein, an injectable in situ forming double-network (DN-I) hydrogel has been developed that can provide mechanical cell protection during injection, support long-term retention postinjection, and be degraded rapidly to allow space for encapsulated cell growth. The hydrogel was cross-linked via a reversible dynamic covalent C═C double bond produced via a Knoevenagel condensation reaction and was further reinforced by in situ UV-induced secondary cross-linking. The dynamic exchange of cross-links in the first network of DN-I hydrogel was significantly enhanced using a biocompatible catalyst, histidine. The large dynamic network of the DN-I hydrogel allowed injection of prefabricated hydrogels with encapsulated cells using less force and provided mechanical protection from the injection forces. The secondary cross-linking network improved the retention of the transplanted cells postinjection and subsequently provided support for cell proliferation and differentiation. The as-developed injectable in situ forming double-network hydrogel can be used as an effective carrier for stem cell transplantation and tissue regeneration applications.

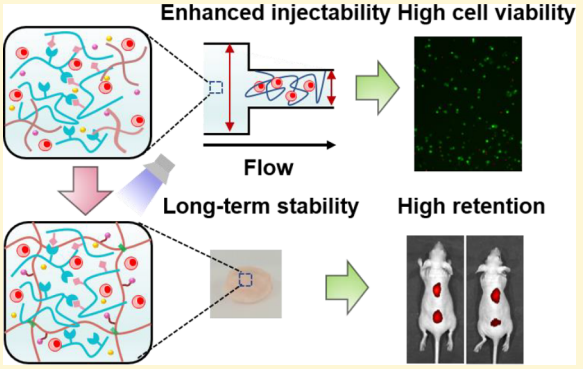

1. INTRODUCTION

Injectable cell transplantation has displayed great potential in the treatment of several injuries and diseases, such as cardiac disease, peripheral nerve injury, and spinal cord injury.[1−5] However, successful cell transplantation is limited by several obstacles.[6−11] First, the transplanted cells are severely damaged through mechanical force-induced cell membrane damages during injection.[12,13] Next, the low cell retention postinjection leads to cell dispersal from the injection site, thus leading to the failure of cell transplantation.[6] Also, the maintenance of proliferation and/or differentiation for transplanted cells is key for cell transplantation, which is believed to be influenced by the in vitro mechanical microenvironment including stiffness,[14,15] material degradation,[16,17] and stress relaxation.[18−20] Thus, there is a great need of novel materials to assist in successful cell transplantation therapy.

Hydrogels are water-swollen and insoluble polymeric networks that are widely used for the controlled delivery of cells and drugs.[21−28] In particular, owing to their shear-thinning and self-healing abilities, injectable hydrogels hold potential in cell transplantation, which can be used to protect the encapsulated cells from mechanical injuries during the injection stage.[29,30] Moreover, rapid self-healing of the hydrogel at the injection site would provide support for the encapsulated cells and prevent post-transplantation cell dispersal. However, most of the injectable hydrogels undergo rapid degradation because of the fast exchange kinetics of cross-linking. The lack of long-term stability results in fast and uncontrolled collapse of the cell scaffold, causing the burst release of cells, which significantly limits the cell transplantation efficacy.[13,16] In contrast, covalently cross-linked hydrogels have stable cross-linking networks and have been reported to provide a stable scaffold for cells.[31,32] However, typically, the covalently cross-linked hydrogels do not allow simple delivery of the material via injection, which significantly limits their potential for use as a cell carrier in cell transplantation. Therefore, combining the advantages of dynamic hydrogels and covalently cross-linked hydrogels to design a double-network hydrogel is promising to improve the cell viability during injection, enhance cell retention post-

Received: February 22, 2021
Revised: July 14, 2021
Published: July 22, 2021

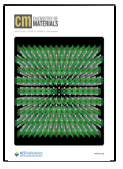

injection, and allow simultaneous cell growth within the hydrogel. However, till date, no hydrogel has addressed all the challenges faced by cell transplantation through local injection.[6,29]

Herein, an injectable in situ forming double-network (DN-I) hydrogel has been designed that can provide mechanical cell protection during injection, support long-term retention postinjection, and be degraded to allow space for the encapsulated cells' proliferation and differentiation. The DN-I hydrogel first underwent gelation through the formation of a dynamic C═C double bond based on the Knoevenagel condensation (KC) reaction by mixing the benzaldehyde and cyanoacetate group-functionalized dextran. Upon exposure to ultraviolet (UV) light, secondary cross-linking occurred via photopolymerization of acrylated 4-arm PEG (4-arm PEG-A) to form an in situ reinforced network (Scheme 1a,b). The obtained DN-I hydrogel displayed superb injectable and self-healing performance owing to the addition of the histidine catalyst (Scheme 1c), which could effectively protect the encapsulated cells from mechanical injuries during injection and provide a temporary scaffold to prevent the cell dispersal.

Scheme 1. Preparation and Chemical Structures of Injectable In Situ Forming Double-Network Hydrogel.

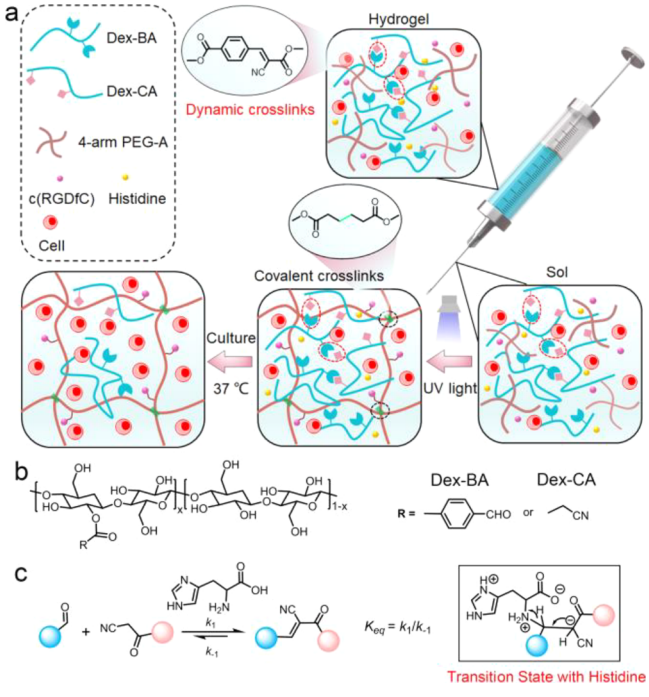

[a](a) Preparation of Injectable In Situ Forming Double-Network Hydrogel. During the injection, the histidine catalyst promotes the rapid exchange of dynamic C═C double bonds and rearrangement of the network to facilitate the flow of hydrogel and protect the encapsulated cells from the mechanical force-induced injuries. After the injection, UV-initiated radical polymerization of the acrylate groups at the end of 4-arm PEG-A led to secondary cross-linking and enhanced retention of the DN-I hydrogel. Furthermore, rapid degradation of the first dynamic network promoted proliferation and differentiation of the encapsulated cells. (b) Chemical structures of cyanoacetate- and benzaldehyde-modified dextran polymers. (c) Schematic of histidine-accelerated dynamic exchanges of C═C double bonds, wherein the catalyst histidine formed a transition state with aldehyde to accelerate dehydration of the rate-determining step.

Moreover, the photocross-linked secondary network provided a long-term stable scaffold to enhance cell retention within the DN-I hydrogel at the target site. Also, the first network could be rapidly degraded via hydrolysis, resulting in the creation of more space within the DN-I hydrogel for cell differentiation and proliferation.

2. EXPERIMENTAL SECTION

2.1 Preparation of Single-Network Injectable (S-I) Hydrogels. Dex-BA and Dex-CA were separately dissolved in Milli-Q water to form stock solutions. The catalyst histidine was dissolved in Milli-Q water at a stock concentration of 10 mg/mL. S-I hydrogels were prepared by mixing Dex-BA and Dex-CA stock solutions at an equal molar ratio of benzaldehyde-to-cyanoacetate group. The concentration of the hydrogel was expressed as a weight (Dex-BA and Dex-CA)/volume percentage (w/v, %). The gelation time of the hydrogel was determined by the time when the sample was not flowing within 30 s after inverting the vital.

2.2 Preparation of DN-I Hydrogels. Dex-BA, Dex-CA, 4-arm PEG-A (5%), and the photoinitiator Irgacure 2959 (0.1%) were first dissolved in 300 μL of Milli-Q water at an equal molar ratio of cyanoacetate-to-benzaldehyde group. Then, the hydrogel formed spontaneously within 5 min after addition of histidine. Subsequently, the hydrogel was irradiated by a UV light (365 nm, 10 mW cm^{-2}) for 5 min to form the second network. The hydrogel concentration was expressed as a weight (Dex-BA, Dex-CA, and 4-arm PEG-A)/volume percentage (w/v, %).

2.3 In Vitro Cell Injection and Quantification of Cell Viability. The cell suspension was first mixed with Dex-BA stock solutions before further mixing with histidine, Dex-CA, and 4-arm PEG-A stock solutions. The hydrogel (8%, containing 4.07% Dex-BA and 3.93% Dex-CA) was formed in a 1 mL insulin syringe fitted with a 29G needle. The hydrogel precursor solution was allowed to gel for 10 min before being injected into the cell culture plate at a flow rate of 1 mL min^{-1}. Cell viabilities were measured using the cell counting kit-8 (CCK-8) assay at 20 min postinjection ($n \geq 3$). In brief, the CCK-8 solution (CCK-8, 1.0 mL, 10% v/v in medium) was added on the gel. After incubation for another 2 h, the absorbance values of the medium on the gel at 450 nm were measured using a Bio-Rad 680 microplate reader. The measurements were performed in triplicate. Also, a fluorescent live−dead staining assay was further carried out to visualize the number of live and dead cells after injection (20 min). In brief, 0.5 mL of phosphate-buffered saline (PBS) solution containing calcein-AM (1 mM) and propidium iodide (PI) (1 mM) was pipetted on each cell gel construct. After 30 min, the labeled cells were observed using a fluorescence microscope (Nikon Eclipse Ti-S, Nikon Instruments Co., Ltd). The live cells were stained green fluorescence with calcein-AM and dead cells showed red fluorescence with PI. The quantified data were obtained using ImageJ software (NIH, v1.8.0) based on the staining images.

To confirm the growth of encapsulated cells in the hydrogel after injection, the hydrogel was irradiated by an UV light (365 nm, 10 mW cm^{-2}) for 5 min after injection to form the secondary network. And then, the cells in the DN-I hydrogel were incubated in Dulbecco's modified Eagle medium (DMEM) for 1, 3, and 5 d. The cell proliferation in the DN-I hydrogel after injection was quantitated by a LIVE/DEAD viability/cytotoxicity kit.

2.4 In Vivo Hydrogel Retention Characterization. Female BALB/c nude mice (6−8 weeks old) were chosen to assess the retention of the DN-I hydrogel in vivo. To track the rapid degradation of the first dynamic network, Dex-CA was labeled with a near-infrared fluorescence dye, Cy7. For in vivo transplantation, the mice were anesthetized with isoflurane, and the mixture solutions (60 μL for each sample) containing Dex-BA, Dex-CA, histidine, 4-arm PEG-A, and Irgacure 2959 were injected subcutaneously via an insulin syringe with a 29 G needle. After 10 min, the hydrogel was irradiated by a UV light (365 nm, 10 mW cm^{-2}) for another 10 min to form the second network. In this experiment, a hydrogel precursor solution without 4-arm PEG-A was used as a control. At different time intervals, the

https://doi.org/10.1021/acs.chemmater.1c00635
Chem. Mater. 2021, 33, 5885−5895

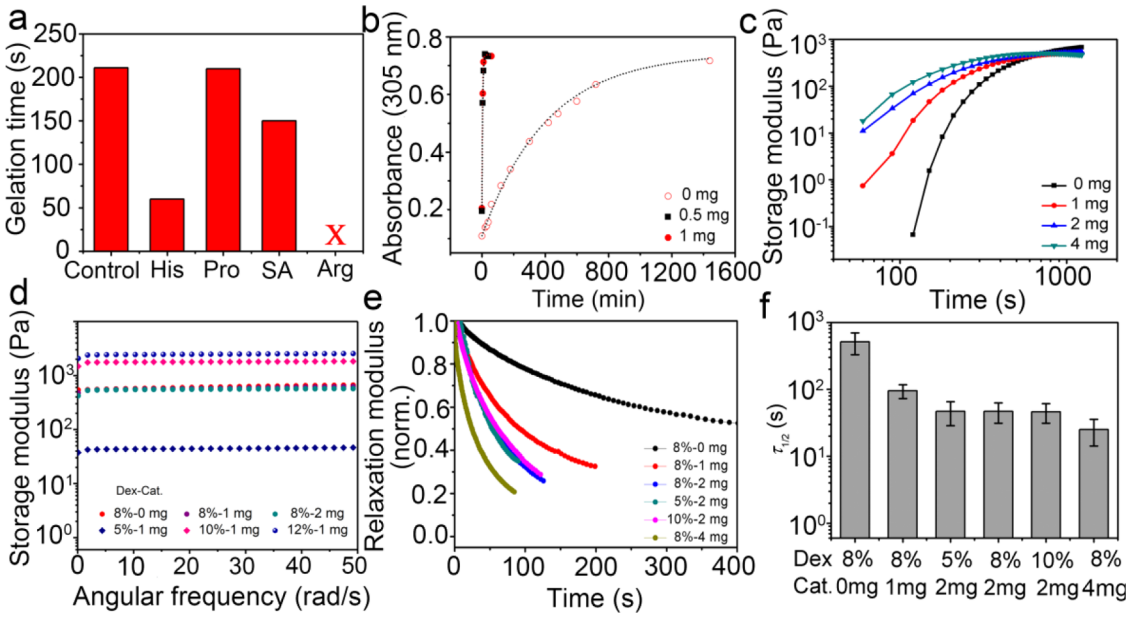

Figure 1. Effect of the histidine catalyst on the reversible C═C double bond exchange reaction and properties of the S-I hydrogel prepared from Dex-BA and Dex-CA in the presence of histidine. (a) Gelation time of 8% S-I hydrogels with the same amount (0.013 mmol) of different catalysts (control group represents the S-I hydrogel formed without a catalyst. His, Pro, and SA groups represent the S-I hydrogels formed in the presence of histidine, proline, and sodium ascorbate, respectively). The red "X" indicates that the S-I hydrogel could not be formed when arginine (Arg) was used as the catalyst. (b) Time-dependent UV−vis absorbance spectra of 5% polymer solutions at 37 °C in Milli-Q water for histidine concentrations of 0 mg, 0.5 mg, and 1 mg. (c) Oscillatory time sweep (8% gel) demonstrating that the gelation was accelerated with rising histidine concentrations but the equilibrium modulus of the hydrogels remained unchanged. (d) Oscillatory frequency sweep demonstrates that the hydrogel modulus was independent of incorporated histidine concentrations but dependent on the dextran concentrations. (e) Stress relaxation was accelerated by the increase of the histidine concentrations but was independent of the dextran concentrations. Relaxation modulus was normalized by the initial relaxation modulus. (f) Quantification of $\tau_{1/2}$ as per stress relaxation tests in panel (e)

retention of the first dynamic hydrogel network was monitored with an in vivo imaging system (Caliper Life Sciences, USA) at day 0, 3, and 7 postinjection, and the data were analyzed using Living Image software (Caliper Life Sciences, USA). To track the long-term retention of the DN-I hydrogel network, thiolated Cy5 was incorporated into the secondary network in the hydrogel. Hydrogel precursor solutions (60 μL for each sample) containing Dex-BA, Dex-CA, histidine, 4-arm PEG-A, and Irgacure 2959 were injected subcutaneously via an insulin syringe with a 29 G needle. After 10 min, the hydrogel was irradiated by a UV light (365 nm, 10 mWcm^{-2}) for another 10 min to form the second network. For this experiment, hydrogel precursor solutions (60 μL for each sample) containing 4-arm PEG-A, thiolated Cy5, and Irgacure 2959 were used as a control. At different time intervals, the retention of the DN-I hydrogel network was monitored with an in vivo imaging system (Caliper Life Sciences, USA) at day 0, 3, 7, 15, and 21 postinjection, and the data were analyzed using Living Image software (Caliper Life Sciences, USA).

3. RESULTS AND DISCUSSION

In our previous work, we have shown that a C═C double bond formed by the catalysis-free Knoevenagel condensation (CKC) reaction between benzaldehyde and cyanoacetate in the aqueous solution was a thermally reversible dynamic covalent bond, which could be used to formulate injectable, self-healing, and thermosensitive hydrogels under physiological conditions.[33,34] However, the dynamic exchanges of the C═C double bond are relatively slow, which results in the hydrogel prepared from the CKC reaction to be not satisfactory for an injectable cell carrier. Fortunately, it has been demonstrated that the KC reaction in aqueous media can be accelerated by multiple biocompatible catalysts, such as sodium ascorbate, histidine, proline, and arginine.[35−37] Therefore, herein, it is proposed that the abovementioned catalysts can be used to accelerate the formation of C═C double bonds, enhance the dynamic exchange, and improve the injectability of hydrogels based on the KC reaction. To verify this hypothesis, a proof-of-concept study was conducted using benzaldehyde and cyanoacetate group-functionalized dextran, denoted as Dex-BA and Dex-CA, respectively, as the model building blocks (Figures S1−S3). The hydrogel readily formed upon mixing Dex-BA and Dex-CA with an equal molar ratio of benzaldehyde-to-cyanoacetate group. The catalytic efficiency of different catalysts in water was investigated by measuring the gelation time of hydrogels using the same amount of catalysts. As shown in Figure 1a and Figure S4, the hydrogel with the histidine catalyst had the lowest gelation time compared to the hydrogels with proline and sodium ascorbate, signifying that histidine exhibits the highest catalytic efficiency for the KC reaction. To illustrate that the exchange of the dynamic C═C double bond can be accelerated by histidine, methoxy poly(ethylene glycol) end-functionalized with benzaldehyde and cyanoacetate, denoted as mPEG-BA and mPEG-CA, respectively, was prepared and used as reactive model compounds to study the histidine-catalyzed KC reaction process (Figure S5). The rate of C═C double bond formation (k_1) and cleavage (k_{-1}) with different contents of histidine was measured, and the equilibrium constant (K_{eq}) was obtained from the reaction rate constants (Table S1). As shown in Figure 1b, histidine exhibited effective catalytic activity for the KC reaction and both k_1 and k_{-1} were significantly accelerated with the rise in the histidine content. K_{eq} of the reaction remained unchanged and was independent of histidine contents. Similarly, a vial inversion test shows that as the

https://doi.org/10.1021/acs.chemmater.1c00635
Chem. Mater. 2021, 33, 5885−5895

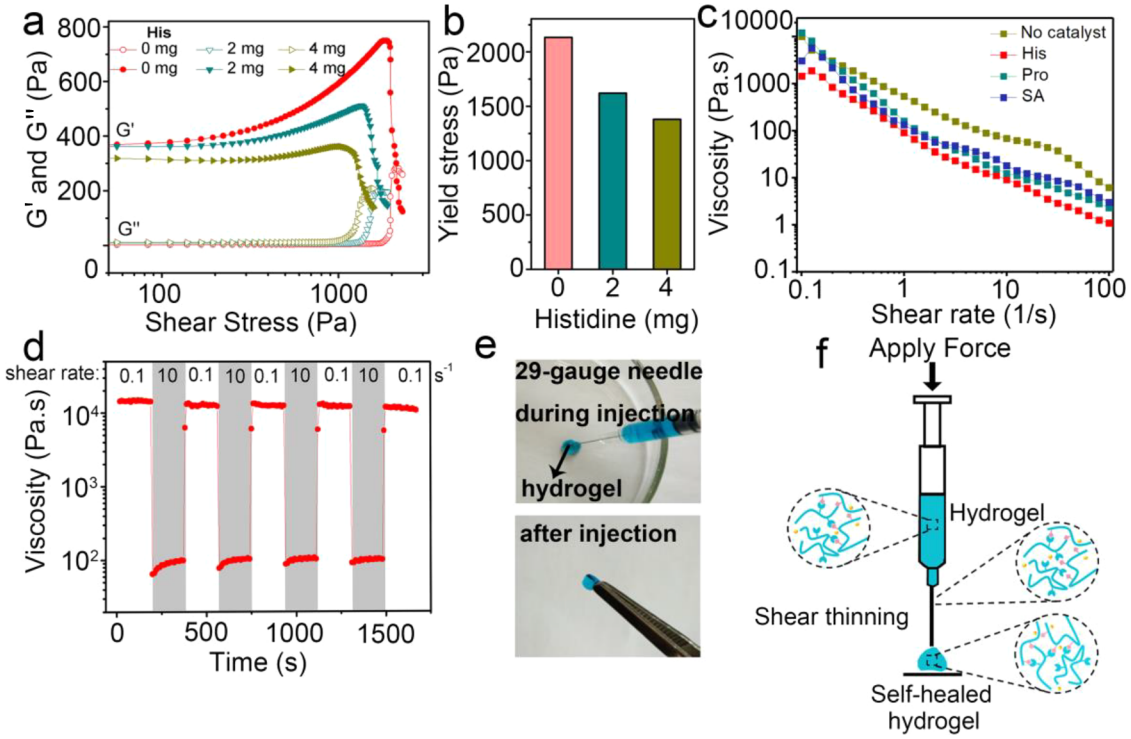

Figure 2. (a) G' and G'' as a function of shear stress for the 8% S-I hydrogel with different histidine contents. (b) Quantification of the yield stress from shear stress sweep tests in panel (a). (c) Viscosity measurements of the 8% S-I hydrogel as a function of shear rate with different catalysts (2 mg) at 37 °C. (d) Shear-thinning and self-healing properties of the 8% S-I hydrogel under alternating shear rates of 0.1 and 10 s^{-1} at 37 °C. (e) Images of the 8% S-I hydrogel to be ejected through a 29 G needle without clogging (the hydrogel was dyed with Coomassie brilliant blue for visualization). (f) Schematic illustration of the injection process for the S-I hydrogel.

concentration of histidine increased from 0 to 4 mg, the gelation time of hydrogels based on the dynamic C═C double bond decreased from 140 to 60 s (Figure S6). Furthermore, the gelation process was evaluated using dynamic time sweep rheological experiments. As shown in Figure 1c, the hydrogels with different histidine contents reached the same final plateau modulus of about 950 Pa and amplifying the histidine loading to 4 mg further shortened the time to 1 min. Thereafter, the mechanical properties of hydrogels were studied using the dynamic frequency sweep tests. Figure 1d shows that G' of the hydrogels with different histidine contents and polymer concentrations reached a plateau in the entire frequency range. G' remained unchanged regardless of the catalyst loading amount at a fixed polymer concentration, which suggests that the catalyst histidine had no effect on the equilibrium network structure or hydrogel modulus. In contrast, when the histidine content was fixed at 1 mg, G' increased significantly with the rise in dextran concentrations. Next, the impact of histidine on the stress relaxation behavior was explored. The stress relaxation rate under a constant strain was defined by the time at which the stress relaxed to half of its original value, $\tau_{1/2}$. As shown in Figure 1e,f, the stress relaxation rate was enhanced significantly for these hydrogels in the presence of histidine, with $\tau_{1/2}$ decreasing from 580 s without histidine to 25 s with 4 mg histidine. However, the stress relaxation rate did not change with the alteration of dextran polymer concentrations, as shown by the same stress-relaxation profiles for 5, 8, and 10% hydrogels in Figure 1e. Hence, these results indicate that the histidine catalyst accelerated the formation and exchange dynamics of the C═C double bond but hardly affected the thermodynamic equilibrium, which could result in improved injectability of the hydrogel.

Hydrogels with rapid exchange dynamics of cross-linking are expected to be ejected using less force, and the applied force for injection is usually determined by the yield stress of the hydrogels.[8,38] As shown in Figure 2a,b, when histidine was incorporated into the system, the S-I hydrogels displayed a prominent yield behavior due to the rapid exchange dynamics of C═C double bond linkage. Also, a lower yield stress was observed when more histidine was used, indicating that less force was needed for the injection through a syringe for the case of hydrogels with more histidine. In addition, Figure 2c shows that the viscosity of the S-I hydrogel with histidine was lower than those of the S-I hydrogels without catalysts or with proline and sodium ascorbate as the catalysts. The viscosity of the S-I hydrogel with histidine decreased with an increase in the shear rate from 0.1 to 100 s^{-1} (Figure 2c), implying that the histidine-catalyzed S-I hydrogel displayed a prominent shear-thinning behavior. Owing to the improved dynamic exchange rate of the C═C double bond in the presence of histidine, the S-I hydrogel is expected to exhibit excellent self-healing properties.[8,39−43] Thus, linear viscosity measurements were performed at alternating low and high shear rates (Figure 2d). When the S-I hydrogel was exposed to a high shear rate (10 s^{-1}) at 37 °C, it demonstrated a sharp yield transition behavior, which resulted in a low viscosity (≈100 Pa·s). However, the viscosity rapidly recovered to the original value when a low shear rate (0.1 s^{-1}) was employed, which was probably due to reformation of the dynamic C═C double bond linkage. Additionally, in a strain amplitude test, G' and G'' of the hydrogel initially remained unchanged when the

https://doi.org/10.1021/acs.chemmater.1c00635
Chem. Mater. 2021, 33, 5885−5895

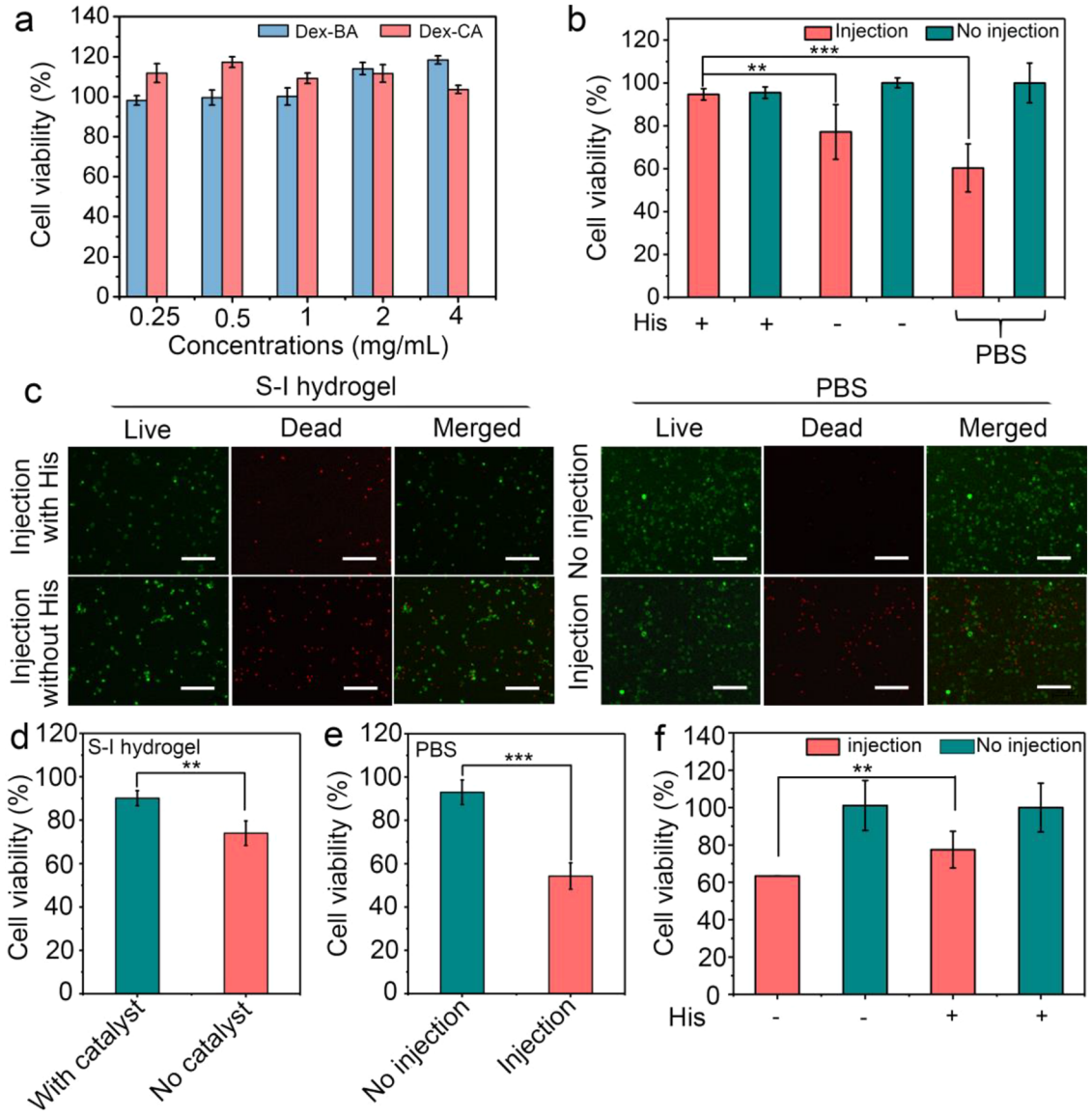

Figure 3. (a) In vitro cytotoxicity of Dex-BA and Dex-CA at different concentrations on HUVECs. (b) HUVEC viability following in vitro injection through a 29 G syringe needle at about 1 mL min^{-1} (**$p < 0.01$, ***$p < 0.001$, $n \geq 3$). (c) Images of LIVE/DEAD analysis for encapsulated HUVECs in S-I hydrogels after injection in the presence and absence of histidine or without injection in the presence of histidine. Scale bar: 50 μm. (d) Quantification of the encapsulated HUVEC viability in the S-I hydrogel immediately after injection in the presence or absence of histidine from the LIVE/DEAD assay shown in panel (c) (**$p < 0.01$, $n \geq 3$). (e) Quantification of the HUVEC viability in PBS solutions with or without injection from the LIVE/DEAD assay shown in panel (c) (***$p < 0.001$, $n \geq 3$). (f) Viability of BMSCs within the 8% S-I hydrogel in the presence and absence of histidine following in vitro injection through a 29 G syringe needle at about 1 mL min^{-1} (**$p < 0.01$, $n \geq 3$).

strain was increased from 1 to 10%. A further increase in the strain to 100% led to a significant drop of both G' and G'' values with a crossover point appearing at about 40% strain, indicating the rupture of the hydrogel network. However, when a small strain of 1% was immediately applied on the destructed hydrogel, it could completely recover to its original mechanical strength (Figure S7). Furthermore, a macroscopic self-healing test was performed to verify the self-healing ability of the S-I hydrogel (Figure S8). Next, the S-I hydrogel was prepared in the barrel of a syringe in the presence of histidine, which could be easily ejected through a 29 G needle without clogging during the injection process. The S-I hydrogels immediately recovered to the gel state after injection (Figure 2e,f) and their modulus remained identical after injection (Figure S9). To conclude, the S-I hydrogel demonstrated excellent injectable and self-healing performance, which are promising for injectable cell delivery applications.

Considering the excellent injectable and self-healing abilities of the S-I hydrogel, the potential of S-I hydrogel to offer mechanical protection for the encapsulated cells during syringe injection was investigated. First, the cytotoxicities of Dex-BA and Dex-CA were evaluated using the MTT assay with human umbilical vein endothelial cells (HUVECs).[44] The cell viabilities of Dex-BA and Dex-CA polymers were all greater than 99% even when their concentrations reached up to 4.0 mg mL^{-1}, suggesting their excellent biocompatibility (Figure 3a and Figure S10). The encapsulated cells in the S-I hydrogel were distributed homogeneously and no aggregation was observed after incubation for 2 h (Figure S11). When the hydrogel was coincubated with HUVECs for 5 days, the

https://doi.org/10.1021/acs.chemmater.1c00635
Chem. Mater. 2021, 33, 5885−5895

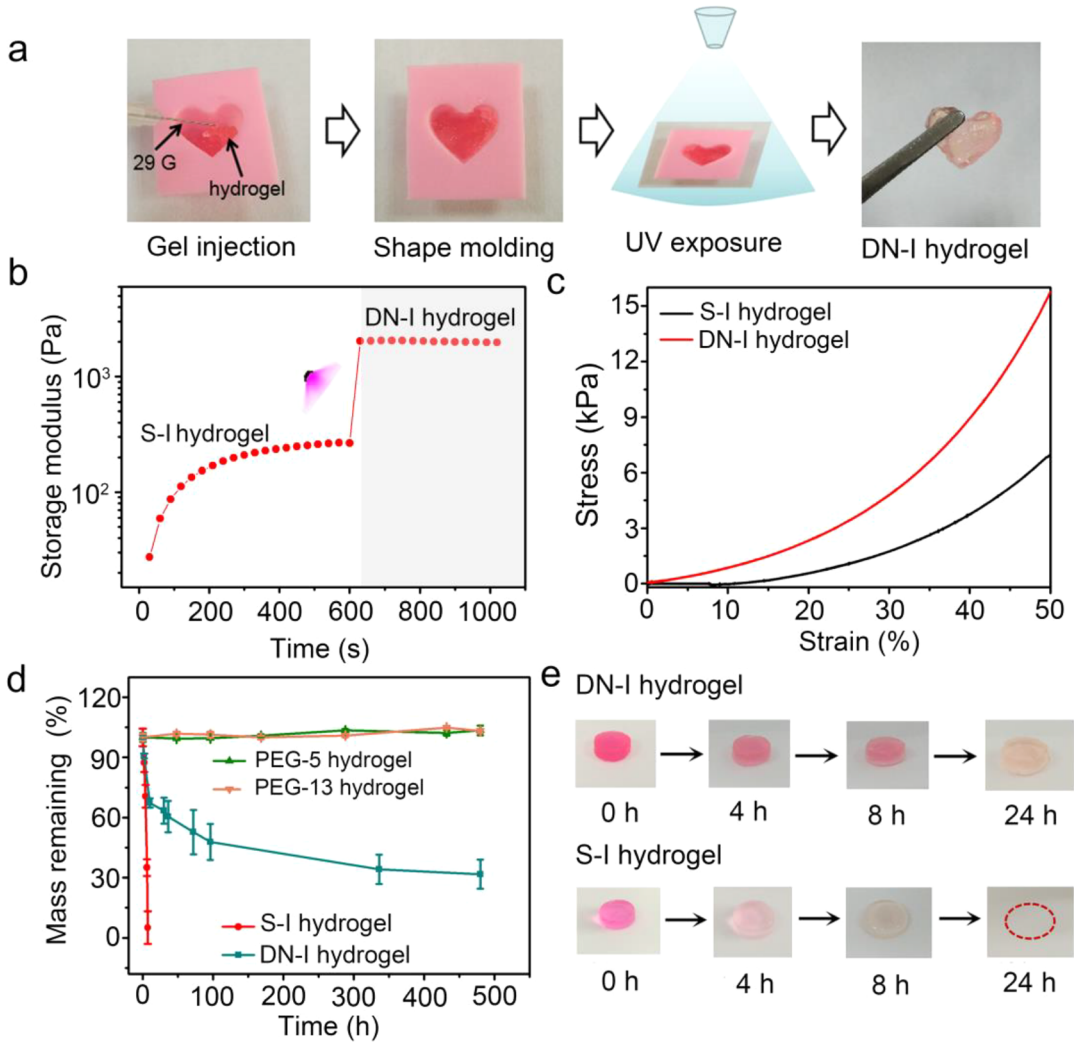

Figure 4. Formation and characterization of the DN-I hydrogel. (a) The 8% S-I hydrogel incorporated with 5% 4-arm PEG-A polymers was injected into a heart-shaped mold and subsequently irradiated by UV light to obtain a heart-shaped DN-I hydrogel. (b) The storage modulus (G') of the 8% S-I hydrogel in the presence of 4-arm PEG-A (5%) polymer as a function of time before and after irradiation with UV light for 5 min at 37 °C. (c) Stress−strain curves of the S-I hydrogel and the DN-I hydrogel. (d) Degradation behaviors of the DN-I hydrogel, S-I hydrogel, PEG-5 (hydrogels formed by UV-cross-linking of 5% 4-arm PEG-A polymer solution), and PEG-13 (hydrogels formed by UV-cross-linking of 13% 4-arm PEG-A solution). (e) Images of the DN-I hydrogel and the S-I hydrogel after swelling in PBS (pH 7.4) for different durations.

majority of cells survived and grew normally (Figure S12). These results demonstrate that the S-I hydrogel formed by the KC reaction had excellent biocompatibility. Next, to confirm the cytoprotective effect of the S-I hydrogel during the injection process, HUVEC suspensions were quickly mixed with the hydrogel precursors containing 2 mg of histidine and the mixture was immediately transferred to a syringe. After the injection, the encapsulated cells were incubated for 20 min and the cell viability was measured using the CCK-8 assay. As shown in Figure 3b, cell viability in the hydrogel after injection was over 90% in the presence of histidine, which showed no difference with the viability of cells directly encapsulated in the S-I hydrogel without injection. In contrast, the injection results in severe cell death with about 77% viability for the hydrogels without histidine, possibly because of the poor injectability of the hydrogels in the absence of histidine.[6,29] Similarly, the cells in a saline solution (PBS, pH 7.4) had a lower cell viability of 56% postinjection. Furthermore, a LIVE/DEAD staining assay was also carried out to test the potential of the S-I hydrogel for use as an injectable cell carrier (Figure 3c−e). The cells delivered with the S-I hydrogel in the presence of histidine exhibited higher viability (90.2 ± 3.5%) compared to the cells encapsulated in the S-I hydrogel without histidine (74 ± 5.6%), while cells delivered with saline solutions exhibited acute cell death (54.3 ± 5.6%). Also, when histidine was incorporated in the hydrogel, the S-I hydrogel demonstrated effective protection for bone marrow mesenchymal stem cells (BMSCs) and maintained their viability up to 80% during injection (Figure 3f). All together, these results indicate that the improved network dynamics of the S-I hydrogel with the histidine catalyst could enhance injectability and meanwhile provide better protection for the cells within the hydrogel during cell transplantation.

Rapid degradation is a major challenge for injectable dynamic hydrogels used as carriers for cell delivery, which largely results in low cell retention at the injection site.[13,16,30,45] To circumvent this drawback, herein, the addition of a second network cross-linked by acrylate-functionalized 4-arm PEG (4-arm PEG-A) (Figures S3 and S13) under UV irradiation has been demonstrated. As shown in Figure 4a, the S-I hydrogel

https://doi.org/10.1021/acs.chemmater.1c00635
Chem. Mater. 2021, 33, 5885−5895

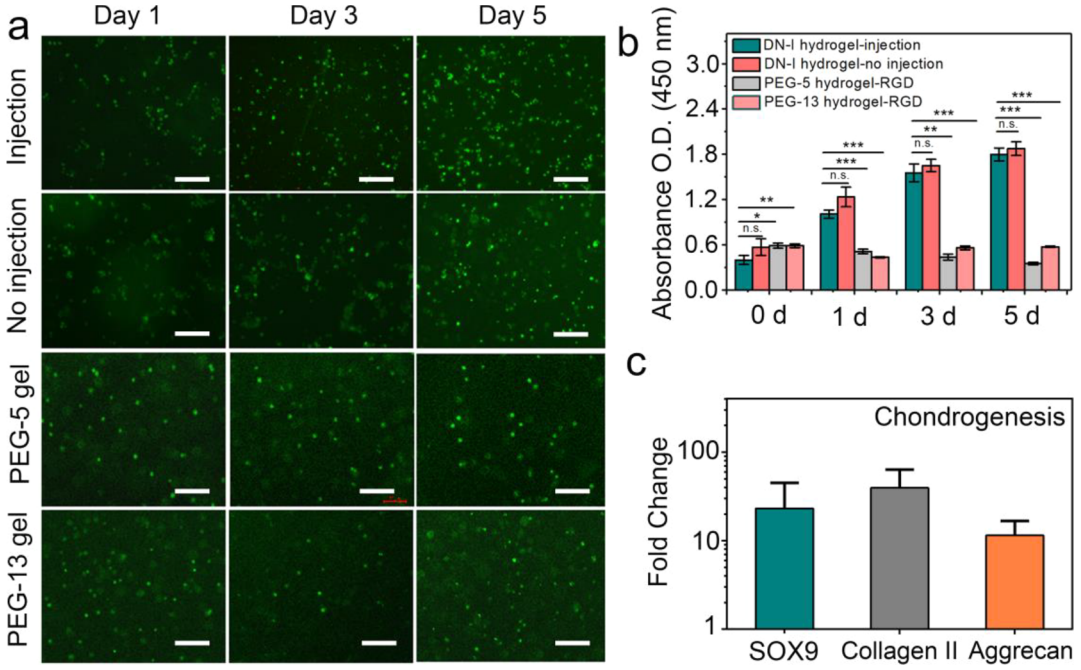

Figure 5. (a) Fluorescence microscopy images of HUVECs cultured within the DN-I hydrogel (with RGD) in the presence or absence of histidine postinjection on days 1, 3, and 5. The PEG-5 hydrogel was cross-linked with 5% 4-arm PEG-A polymers and the PEG-13 hydrogel was cross-linked with 13% 4-arm PEG-A polymers. Scale bar: 50 μm. (b) Proliferation of HUVECs within the DN-I hydrogel with or without histidine postinjection after incubation in DMEM for 1 day, 3 days, and 5 days (*p < 0.05, **p < 0.01, ***p < 0.001, $n \geq 3$). (c) Quantitative gene expression of chondrogenic markers SOX9, collagen II, and aggrecan at day 15. BMSCs were incubated within the DN-I hydrogel in chondrogenic media for 2 weeks. Values are normalized to the gene expression level at day 1.

with 4-arm PEG-A polymers was readily injected into a heart-shaped mold and modeled for 20 min. Subsequently, UV irradiation was applied to the hydrogel for 5 min and a stable heart-shaped hydrogel was obtained. Following the photocross-linking, the storage modulus (G') of the hydrogel increased from ≈266 to ≈2050 Pa, that is, about 8 times (Figure 4b). These results are a strong evidence for the formation of the secondary chemical covalent network resulting from the UV-induced cross-linking of acrylate groups in 4-arm PEG-A. The formation of secondary cross-linking also made the hydrogels more rigid, exhibiting a higher compressive stress at 50% strain (Figure 4c). Young's moduli, calculated from the initial linear region of the stress−strain curves, for DN-I hydrogel and S-I hydrogel were ∼12.4 and ∼3.5 kPa, respectively (Figure S14). The higher Young's modulus of the DN-I hydrogel compared to the S-I hydrogel can be attributed to the formation of an additional secondary network in the DN-I hydrogel. The degradation behavior was then investigated. The S-I hydrogel formed by only dynamic C═C double bonds (i.e., pre-UV exposure) underwent rapid degradation in PBS solutions and no hydrogel mass was retained after 24 h (Figure 4d). The DN-I hydrogel (i.e., post-UV exposure) exhibited initial rapid degradation (50 ± 4% for S-I hydrogel) and subsequent erosion at negligible rates for weeks (Figure 4d). Moreover, with the rise in the histidine concentration, the degradation rate increased (Figure S15). The rapid degradation was likely due to the fast erosion of the dynamic gel network with improved exchange dynamics in the presence of the histidine catalyst. Similarly, G' of the DN-I hydrogel decreased sharply at first owing to the degradation of the first network but remained constant afterward (Figure S16). The integrity of the DN-I hydrogel was maintained after swelling, while the S-I hydrogel was completely dissolved in 24 h of incubation in PBS buffer (Figure 4e). A porous structure of the DN-I hydrogel was observed after swelling for 1 day and 5 days (Figure S17). These results indicate that the stability of the S-I hydrogel was significantly improved due to formation of the secondary network and rapid degradation of the first dynamic network in the DN-I hydrogel allowing more space for differentiation and proliferation of the encapsulated cells.

To study the potential of the DN-I hydrogel for use as an injectable cell carrier, cell viability after injection was measured using a LIVE/DEAD cell staining assay. To enhance the cell affinity in the hydrogel, a cell-adhesive RGD peptide was added into the DN-I hydrogel via Michael-type addition between the acrylate groups from 4-arm PEG-A and thiolated RGD peptide under physiological conditions (Figure S18). HUVECs were encapsulated within the RGD-modified DN-I hydrogels with 2 mg of histidine. HUVECs were injected through a 29 G needle into a Petri dish, subsequently irradiated using UV light (365 nm, 10 mW cm^{-2}) for 5 min, and cultured under physiological conditions in DMEM for different days. As shown in Figure 5a,b, the LIVE/DEAD staining assay demonstrates that HUVECs cultured in the injectable DN-I hydrogel remained proliferative with a homogeneous cell distribution and minimal dead cells postinjection, which is similar to the viability of cells encapsulated in the DN-I hydrogels without injection. In contrast, the proliferation behavior of HUVECs within the covalent PEG-5 hydrogel and PEG-13 hydrogel was clearly suppressed after the injection and in vitro incubation for 5 days, possibly due to the static nature of these two covalent hydrogels.[46,47] These results suggest that the encapsulated cells in the DN-I hydrogel retained their proliferation ability after injection. A possible reason for the phenomenon is that the rapid degradation of the first dynamic network resulted in the creation of more space within the DN-I hydrogel for cell

https://doi.org/10.1021/acs.chemmater.1c00635
Chem. Mater. 2021, 33, 5885−5895

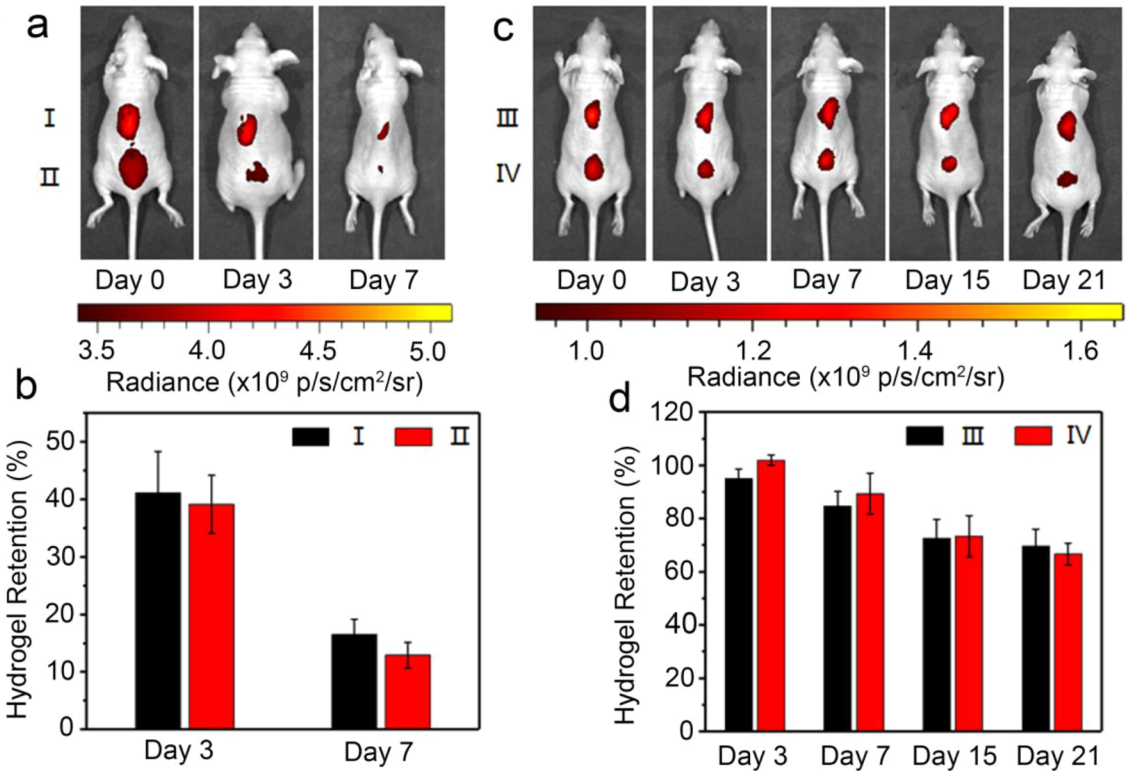

Figure 6. Hydrogel retention after in vivo subcutaneous injection. (a) Fluorescence images of hydrogels labeled with a near-infrared fluorescence dye, Cy7, at 0, 3, and 7 days after injection. I represents the DN-I hydrogel without UV irradiation and II represents the S-I hydrogel. (b) Quantification of material retention relative to day 0 in panel (a). (c) Fluorescence images of hydrogels labeled with a near-infrared fluorescence dye, Cy5, at 0, 3, 7, 15, and 21 days after injection. III represents the DN-I hydrogel with UV irradiation for 10 min and IV represents the covalent PEG-5 hydrogel. (d) Quantification of hydrogel retention relative to day 0 in panel (c).

proliferation after injection. Another reason may be that the rate of stress relaxation for the DN-I hydrogel was markedly enhanced by histidine.[48,49] In order to confirm these hypotheses, stress relaxation tests of DN-I hydrogel and a covalently cross-linked 4-arm PEG-A hydrogel were performed (Figure S19). The DN-I hydrogel exhibited a similar stress-relaxation behavior as that of the dynamic S-I hydrogel. In contrast, a negligible stress-relaxation behavior was observed for the covalently cross-linked hydrogel. Furthermore, to evaluate the ability of the DN-I hydrogel to maintain long-term cell viability and differentiation after injection, BMSCs were encapsulated in the hydrogel, injected through a 29 G syringe needle, and then were cultured for up to 2 weeks in the chondrogenic media. On day 15, the level of gene expression of chondrogenic markers including SOX9, type II collagen (COL-II), and aggrecan was measured via reverse-transcription quantitative PCR, with glyceraldehyde-3-phosphate dehydrogenase as a housekeeping gene. SOX9, COL-II, and aggrecan are established as the major extracellular components of cartilage and are used as indicators of chondrogenesis.,[50,51] As shown in Figure 5c, the relative gene expression levels of SOX9, COL-II, and aggrecan exhibited a 15-, 38-, and 11-fold increase, respectively, compared to those on day 1. Therefore, BMSC cells encapsulated within the DN-I hydrogel maintained the potential to differentiate after injection. Hence, it can be concluded that the DN-I hydrogel after injection could provide a suitable dynamic scaffold for cell proliferation and differentiation in vitro.

Next, the improved retention of the DN-I hydrogel in vivo was evaluated. The hydrogels were injected subcutaneously into nude mice through a 29 G needle and rapidly recovered as a compact gel, which was visible and obvious as small bumps at the injection site. Dex-CA was labeled with a near-infrared fluorescence dye, Cy7 (Figure S20a), prior to the injection to observe rapid degradation of the first dynamic network (Figure 6a). On day 7, about 16 and 12% of the hydrogel material was retained for the DN-I hydrogel without receiving UV light and S-I hydrogel, respectively (Figure 6b), suggesting that the first dynamic network underwent rapid degradation in vivo. For the DN-I hydrogel, immediately after the formation of the first network, it was exposed to UV irradiation for 10 min to form the second network (Figure 6c). The covalent hydrogel that was only cross-linked with 4-arm PEG-A was included as a control (Figure 6c). Hydrogel retentions were tracked noninvasively by incorporating a near-infrared fluorescence dye, thiolated Cy5, into the hydrogel (Figure S20b). On day 21, the remaining materials of the DN-I hydrogel and PEG-5 hydrogel were about 69 and 66%, respectively (Figure 6d), which indicates that the stability of DN-I hydrogel was significantly enhanced after the addition of the secondary network. Collectively, these results indicate that the addition of a secondary network can effectively promote the long-term retention of the DN-I hydrogel at the target site.

4. CONCLUSIONS

In summary, an in situ forming double-network hydrogel with remarkable injectable and long-term retention properties has been prepared. The hydrogels first underwent gelation through the formation of dynamic C═C double bonds based on the KC reaction and were further cross-linked via photopolyme-

https://doi.org/10.1021/acs.chemmater.1c00635
Chem. Mater. 2021, 33, 5885−5895

rization of acrylate groups in 4-arm PEG-A polymers. The dynamic hydrogel displayed great injectability with the use of a biocompatible catalyst histidine that enhanced the exchange dynamics of the C═C double bond in the dynamic network. Hence, such hydrogels could effectively protect the cells from mechanical damage during injection and provide a temporary scaffold for postinjection cell retention owing to the rapid self-healing ability of the first dynamic network. Furthermore, the photocross-linked network in the double-network hydrogel enhanced the retention of the DN-I hydrogel at the target site and further provided a stable scaffold for long-term cell proliferation and differentiation. Therefore, the as-developed injectable in situ forming double-network hydrogel can be used for stem cell transplantation and tissue regeneration applications.

■ ASSOCIATED CONTENT

Supporting Information

The Supporting Information is available free of charge at https://pubs.acs.org/doi/10.1021/acs.chemmater.1c00635.

Detailed materials and additional experimental methods; ^{1}H and ^{13}C NMR spectra of Dex-BA, Dex-CA, and 4-arm PEG-A; ^{1}H NMR spectra of mPEG-BA and mPEG-CA; FTIR spectra of Dex-BA, Dex-CA, and 4-arm PEG-A; gelation times of the S-I hydrogel with different kinds of catalysts; in vitro degradation; compressive tests of the DN-I hydrogel and S-I hydrogel; reaction rates and equilibrium constants between mPEG-BA and mPEG-CA, self-healing properties of the S-I hydrogel; SEM images of the DN-I hydrogel; CLSM images of HUVECs encapsulated in the S-I hydrogel; Live/Dead staining experiments; proliferation rate of HUVECs within the DN-I hydrogel; relaxation modulus of hydrogels; and chemical structures of Dex-BA and Dex-CA labeled with near-infrared fluorescence dyes (PDF)

■ AUTHOR INFORMATION

Corresponding Authors

Gao Li − *Key Laboratory of Polymer Ecomaterials, Changchun Institute of Applied Chemistry, Chinese Academy of Sciences, Changchun 130022, China; University of Science and Technology of China, Hefei 230026, China;* orcid.org/0000-0003-1171-9179; Email: ligao@ciac.ac.cn

Tianmeng Sun − *International Center of Future Science, Institute of Immunology, The First Hospital, Jilin University, Changchun 130061, China;* orcid.org/0000-0003-2261-4532; Email: tsun41@jlu.edu.cn

Chunsheng Xiao − *Key Laboratory of Polymer Ecomaterials, Changchun Institute of Applied Chemistry, Chinese Academy of Sciences, Changchun 130022, China; Jilin Biomedical Polymers Engineering Laboratory, Changchun 130022, China;* orcid.org/0000-0001-7936-4146; Email: xiaocs@ciac.ac.cn

Authors

Xiaoya Ding − *Key Laboratory of Polymer Ecomaterials, Changchun Institute of Applied Chemistry, Chinese Academy of Sciences, Changchun 130022, China; University of Science and Technology of China, Hefei 230026, China*

Ye Wang − *International Center of Future Science, Institute of Immunology, The First Hospital, Jilin University, Changchun 130061, China*

Jiaying Liu − *Key Laboratory of Polymer Ecomaterials, Changchun Institute of Applied Chemistry, Chinese Academy of Sciences, Changchun 130022, China; University of Science and Technology of China, Hefei 230026, China*

Peng Zhang − *Key Laboratory of Polymer Ecomaterials, Changchun Institute of Applied Chemistry, Chinese Academy of Sciences, Changchun 130022, China; Jilin Biomedical Polymers Engineering Laboratory, Changchun 130022, China*

Complete contact information is available at: https://pubs.acs.org/10.1021/acs.chemmater.1c00635

Author Contributions

All authors have given approval to the final version of the manuscript.

Funding

This work was financially supported by the National Natural Science Foundation of China (Nos. 51773196, 51973220, 51833010, and 81871478) and the Youth Innovation Promotion Association of Chinese Academy of Sciences (No. 2017266).

Notes

The authors declare no competing financial interest.

■ ABBREVIATIONS

DN-I, Injectable in situ forming double - network; KC, Knoevenagel condensation; CKC, Catalysis-free Knoevenagel condensation; S-I, Single-network injectable hydrogel.

■ REFERENCES

(1) Gage, F. H. Cell therapy. *Nature* **1998**, *30*, 18−24.

(2) Segers, V. F. M.; Lee, R. T. Stem-cell therapy for cardiac disease. *Nature* **2008**, *451*, 937−942.

(3) Shah, N. J.; Mao, A. S.; Shih, T. Y.; Kerr, M. D.; Sharda, A.; Raimondo, T. M.; Weaver, J. C.; Vrbanac, V. D.; Deruaz, M.; Tager, A. M.; Mooney, D. J.; Scadden, D. T. An injectable bone marrow−like scaffold enhances T cell immunity after hematopoietic stem cell transplantation. *Nat. Biotechnol.* **2019**, *37*, 293−302.

(4) Luo, Z.; Pan, J.; Sun, Y.; Zhang, S.; Yang, Y.; Liu, H.; Li, Y.; Xu, X.; Sui, Y.; Wei, S. Injectable 3D Porous Micro-Scaffolds with a Bio-Engine for Cell Transplantation and Tissue Regeneration. *Adv. Funct. Mater.* **2018**, *28*, No. 1804335.

(5) Mitrousis, N.; Fokina, A.; Shoichet, M. S. Biomaterials for cell transplantation. *Nat. Rev. Mater.* **2018**, *3*, 441−456.

(6) Foster, A. A.; Marquardt, L. M.; Heilshorn, S. C. The diverse roles of hydrogel mechanics in injectable stem cell transplantation. *Curr. Opin. Chem. Eng.* **2017**, *15*, 15−23.

(7) Wang, X.; Rivera-Bolanos, N.; Jiang, B.; Ameer, G. A. Advanced functional biomaterials for stem cell delivery in regenerative engineering and medicine. *Adv. Funct. Mater.* **2019**, *29*, No. 1809009.

(8) Lou, J.; Liu, F.; Lindsay, C. D.; Chaudhuri, O.; Heilshorn, S. C.; Xia, Y. Dynamic Hyaluronan Hydrogels with Temporally Modulated High Injectability and Stability Using a Biocompatible Catalyst. *Adv. Mater.* **2018**, *30*, No. 1705215.

(9) Farina, M.; Alexander, J. F.; Thekkedath, U.; Ferrari, M.; Grattoni, A. Cell encapsulation: Overcoming barriers in cell transplantation in diabetes and beyond. *Adv. Drug Delivery Rev.* **2019**, *139*, 92−115.

(10) Sneddon, J. B.; Tang, Q.; Stock, P.; Bluestone, J. A.; Roy, S.; Desai, T.; Hebrok, M. Stem Cell Therapies for Treating Diabetes: Progress and Remaining Challenges. *Cell Stem Cell* **2018**, *22*, 810−823.

(11) Paez-Mayorga, J.; Capuani, S.; Hernandez, N.; Farina, M.; Chua, C. Y. X.; Blanchard, R.; Sizovs, A.; Liu, H. C.; Fraga, D. W.; Niles, J. A.; Salazar, H. F.; Corradetti, B.; Sikora, A. G.; Kloc, M.; Li, X. C.; Gaber, A. O.; Nichols, J. E.; Grattoni, A. Neovascularized implantable cell homing encapsulation platform with tunable local immunosuppressant delivery for allogeneic cell transplantation. *Biomaterials* **2020**, *257*, No. 120232.
(12) Madl, C. M.; Heilshorn, S. C.; Blau, H. M. Bioengineering strategies to accelerate stem cell therapeutics. *Nature* **2018**, *557*, 335−342.
(13) Aguado, B. A.; Mulyasasmita, W.; Su, J.; Lampe, K. J.; Heilshorn, S. C. Improving viability of stem cells during syringe needle flow through the design of hydrogel cell carriers. *Tissue Eng. A* **2012**, *18*, 806−815.
(14) Lam, J.; Carmichael, S. T.; Lowry, W. E.; Segura, T. Hydrogel Design of Experiments Methodology to Optimize Hydrogel for iPSC-NPC Culture. *Adv. Healthcare Mater.* **2015**, *4*, 534−539.
(15) Quarta, M.; Brett, J. O.; DiMarco, R.; De Morree, A.; Boutet, S. C.; Chacon, R.; Gibbons, M. C.; Garcia, V. A.; Su, J.; Shrager, J. B.; Heilshorn, S.; Rando, T. A. An artificial niche preserves the quiescence of muscle stem cells and enhances their therapeutic efficacy. *Nat. Biotechnol.* **2016**, *34*, 752−759.
(16) Shen, W.; Zhang, K.; Kornfield, J. A.; Tirrell, D. A. Tuning the erosion rate of artificial protein hydrogels through control of network topology. *Nat. Mater.* **2006**, *5*, 153−158.
(17) Martens, P. J.; Bryant, S. J.; Anseth, K. S. Tailoring the Degradation of Hydrogels Formed from Multivinyl Poly(ethylene glycol) and Poly(vinyl alcohol) Macromers for Cartilage Tissue Engineering. *Biomacromolecules* **2003**, *4*, 283−292.
(18) Chaudhuri, O.; Gu, L.; Klumpers, D.; Darnell, M.; Bencherif, S. A.; Weaver, J. C.; Huebsch, N.; Lee, H. P.; Lippens, E.; Duda, G. N.; Mooney, D. J. Hydrogels with tunable stress relaxation regulate stem cell fate and activity. *Nat. Mater.* **2016**, *15*, 326−334.
(19) Nam, S.; Stowers, R.; Lou, J.; Xia, Y.; Chaudhuri, O. Varying PEG density to control stress relaxation in alginate-PEG hydrogels for 3D cell culture studies. *Biomaterials* **2019**, *200*, 15−24.
(20) Yang, M.; Xu, Z.; Li, P.; Guo, F.; Liu, Y.; Xiao, Y.; Gao, W.; Gao, C. Interlayer crosslinking to conquer the stress relaxation of graphene laminated materials. *Mater. Horiz.* **2018**, *5*, 1112−1119.
(21) Peppas, N. A.; Hilt, J. Z.; Khademhosseini, A.; Langer, R. Hydrogels in Biology and Medicine: From Molecular Principles to Bionanotechnology. *Adv. Mater.* **2006**, *18*, 1345−1360.
(22) Tibbitt, M. W.; Anseth, K. S. Hydrogels as Extracellular Matrix Mimics for 3D Cell Culture. *Biotechnol. Bioeng.* **2009**, *103*, 655−663.
(23) Drury, J. L.; Mooney, D. J. Hydrogels for tissue engineering: scaffold design variables and applications. *Biomaterials* **2003**, *24*, 4337−4351.
(24) Ma, W.; Chen, Q.; Xu, W.; Yu, M.; Yang, Y.; Zou, B.; Zhang, Y. S.; Ding, J.; Yu, Z. Self-targeting visualizable hyaluronate nanogel for synchronized intracellular release of doxorubicin and cisplatin in combating multidrug-resistant breast cancer. *Nano Res.* **2021**, *14*, 846−857.
(25) Ding, X. Y.; Wang, Y.; Li, G.; Xiao, C. S.; Chen, X. S. Iminoboronate Ester Cross-linked Hydrogels with Injectable, Self-healing and Multi-responsive Properties. *Acta Polym. Sin.* **2019**, *50*, 505−515.
(26) Martin, J. R.; Patil, P.; Yu, F.; Gupta, M. K.; Duvall, C. L. Enhanced stem cell retention and antioxidative protection with injectable, ROS-degradable PEG hydrogels. *Biomaterials* **2020**, *263*, No. 120377.
(27) Wang, X.; Wang, C.; Wang, X.; Wang, Y.; Zhang, Q.; Cheng, Y. A Polydopamine Nanoparticle-Knotted Poly(ethylene glycol) Hydrogel for On-Demand Drug Delivery and Chemo-photothermal Therapy. *Chem. Mater.* **2017**, *29*, 1370−1376.
(28) Mao, Q.; Hoffmann, O.; Yu, K.; Lu, F.; Lan, G.; Dai, F.; Shang, S.; Xie, R. Self-contracting oxidized starch/gelatin hydrogel for noninvasive wound closure and wound healing. *Mater. Des.* **2020**, *194*, No. 108916.
(29) Marquardt, L. M.; Heilshorn, S. C. Design of injectable materials to improve stem cell transplantation. *Curr. Stem Cell Rep.* **2016**, *2*, 207−220.
(30) Li, Y.; Rodrigues, J.; Tomás, H. Injectable and biodegradable hydrogels: gelation, biodegradation and biomedical applications. *Chem. Soc. Rev.* **2012**, *41*, 2193−2221.
(31) Ferreira, L. S.; Gerecht, S.; Fuller, J.; Shieh, H. F.; Vunjak-Novakovic, G.; Langer, R. Bioactive hydrogel scaffolds for controllable vascular differentiation of human embryonic stem cells. *Biomaterials* **2007**, *28*, 2706−2717.
(32) Mann, B. K.; Gobin, A. S.; Tsai, A. T.; Schmedlen, R. H.; West, J. L. Smooth muscle cell growth in photopolymerized hydrogels with cell adhesive and proteolytically degradable domains: synthetic ECM analogs for tissue engineering. *Biomaterials* **2001**, *22*, 3045−3051.
(33) Ding, X.; Li, G.; Zhang, P.; Xiao, C. Constructing Thermally Reversible Dynamic Hydrogels via Catalysis-Free Knoevenagel Condensation. *ACS Macro Lett.* **2020**, *9*, 830−835.
(34) Ding, X.; Li, G.; Zhang, P.; Jin, E.; Xiao, C.; Chen, X. Injectable Self-Healing Hydrogel Wound Dressing with Cysteine-Specific On-Demand Dissolution Property Based on Tandem Dynamic Covalent Bonds. *Adv. Funct. Mater.* **2021**, *31*, No. 2011230.
(35) Bigi, F.; Quarantelli, C. The Knoevenagel Condensation in Water. *Curr. Org. Synth.* **2012**, *9*, 31−39.
(36) Rahmati, A.; Vakili, K. L-Histidine and L-arginine promote Knoevenagel reaction in water. *Amino Acids* **2010**, *39*, 911−916.
(37) Kiyani, H.; Ghorbani, F. Sodium Ascorbate as Green and Efficient Catalyst for Knoevenagel Condensation of Aryl Aldehydes with Meldrum's Acid in Aqueous Media. *Jordan J. Chem.* **2013**, *8*, 191−198.
(38) Wei, Q.; Xu, M.; Liao, C.; Wu, Q.; Liu, M.; Zhang, Y.; Wu, C.; Cheng, L.; Wang, Q. Printable hybrid hydrogel by dual enzymatic polymerization with superactivity. *Chem. Sci.* **2016**, *7*, 2748−2752.
(39) de Alwis Watuthanthrige, N.; Ahammed, B.; Dolan, M. T.; Fang, Q. H.; Wu, J.; Sparks, J. L.; Zanjani, M. B.; Konkolewicz, D.; Ye, Z. Accelerating dynamic exchange and self-healing using mechanical forces in crosslinked polymers. *Mater. Horiz.* **2020**, *7*, 1581−1587.
(40) Li, Y.; Yang, L.; Zeng, Y.; Wu, Y.; Wei, Y.; Tao, L. Self-Healing Hydrogel with a Double Dynamic Network Comprising Imine and Borate Ester Linkages. *Chem. Mater.* **2019**, *31*, 5576−5583.
(41) Ding, X.; Li, G.; Xiao, C.; Chen, X. Enhancing the Stability of Hydrogels by Doubling the Schiff Base Linkages. *Macromol. Chem. Phys.* **2019**, *220*, No. 1800484.
(42) Tran, V. T.; Mredha, M. T. I.; Na, J. Y.; Seon, J.-K.; Cui, J.; Jeon, I. Multifunctional poly(disulfide) hydrogels with extremely fast self-healing ability and degradability. *Chem. Eng. J.* **2020**, *394*, No. 124941.
(43) Zhao, X.; Wu, H.; Guo, B.; Dong, R.; Qiu, Y.; Ma, P. Antibacterial anti-oxidant electroactive injectable hydrogel as self-healing wound dressing with hemostasis and adhesiveness for cutaneous wound healing. *Biomaterials* **2017**, *122*, 34−47.
(44) Asweto, C.; Wu, J.; Hu, H.; Feng, L.; Yang, X.; Duan, J.; Sun, Z. Combined Effect of Silica Nanoparticles and Benzo[a]pyrene on Cell Cycle Arrest Induction and Apoptosis in Human Umbilical Vein Endothelial Cells. *Int. J. Environ. Res. Public Health* **2017**, *14*, 289.
(45) Feng, Q.; Xu, J.; Zhang, K.; Yao, H.; Zheng, N.; Zheng, L.; Wang, J.; Wei, K.; Xiao, X.; Qin, L.; Bian, L. Dynamic and Cell-Infiltratable Hydrogels as Injectable Carrier of Therapeutic Cells and Drugs for Treating Challenging Bone Defects. *ACS Cent. Sci.* **2019**, *5*, 440−450.
(46) Patel, P. N.; Gobin, A. S.; West, J. L.; Patrick, C. W. Poly (ethylene glycol) hydrogel system supports preadipocyte viability, adhesion, and proliferation. *Tissue Eng.* **2005**, *11*, 1498−1505.
(47) Kloxin, A. M.; Kasko, A. M.; Salinas, C. N.; Anseth, K. S. Photodegradable hydrogels for dynamic tuning of physical and chemical properties. *Science* **2009**, *324*, 59−63.
(48) Lou, J.; Stowers, R.; Nam, S.; Xia, Y.; Chaudhuri, O. Stress relaxing hyaluronic acid-collagen hydrogels promote cell spreading, fiber remodeling, and focal adhesion formation in 3D cell culture. *Biomaterials* **2018**, *154*, 213−222.

https://doi.org/10.1021/acs.chemmater.1c00635
Chem. Mater. 2021, 33, 5885−5895

(49) Bauer, A.; Gu, L.; Kwee, B.; Li, W. A.; Dellacherie, M.; Celiz, A. D.; Mooney, D. J. Hydrogel substrate stress-relaxation regulates the spreading and proliferation of mouse myoblasts. *Acta Biomater.* **2017**, *62*, 82−90.
(50) Gosset, M.; Berenbaum, F.; Thirion, S.; Jacques, C. Primary culture and phenotyping of murine chondrocytes. *Nat. Protoc.* **2008**, *3*, 1253−1260.
(51) Feng, Q.; Li, Q.; Wen, H.; Chen, J.; Liang, M.; Huang, H.; Lan, D.; Dong, H.; Cao, X. Injection and Self-Assembly of Bioinspired Stem Cell-Laden Gelatin/Hyaluronic Acid Hybrid Microgels Promote Cartilage Repair In Vivo. *Adv. Funct. Mater.* **2019**, No. 1906690.

https://doi.org/10.1021/acs.chemmater.1c00635
Chem. Mater. 2021, 33, 5885−5895